Demonstration of a Tunable Coupler Suitable for Investigating Ultra-strong Coupling Light-matter Interactions in Superconducting Devices

by

Noah Janzen

A thesis
presented to the University of Waterloo
in fulfillment of the
thesis requirement for the degree of
Master of Science
in
Physics

Waterloo, Ontario, Canada, 2022

Author's Declaration

I hereby declare that I am the sole author of this thesis. This is a true copy of the thesis, including any required final revisions, as accepted by my examiners.

I understand that my thesis may be made electronically available to the public.

Abstract

One of the most ubiquitous processes in nature is the interaction of matter and an electromagnetic field which is well described using the spin-boson model. These light-matter interactions are specified by an interaction strength which is nominally fixed by nature. However, superconducting circuits are able to devise systems using microfabricated quantum devices to increase the dimensionless coupling strength α. The coupling strength is defined as $\alpha = \Gamma_{01}/\pi\Delta$ where Γ_{01} is the decay rate and Δ is the transition frequency of the system. As the strength increases and the rate of interaction approaches the frequency of the system, the light-matter interactions enter the ultra-strong coupling (USC) regime where $\alpha \sim 0.1$. Approximations that are often made to simplify the spin-boson model begin to break down in the USC regime making the analysis of these systems challenging. We demonstrate a flux tunable coupler with potential to explore these dynamics by coupling a persistent current qubit (PCQ) as artificial atom to an open transmission line (TL) as source of continuous bosonic modes. The tunable coupler is able to both decouple the PCQ from the TL as well as enable the USC regime of interactions with a coupling range spanning from $\alpha_{\min} = 2.4 \times 10^{-4}$ to $\alpha_{\max} = 1.2 \times 10^{-1}$. The future objective is to directly explore the time-domain properties of the USC regime and to open new research approaches to relativistic quantum information (RQI) by using the tunable coupler as a switching function.

Acknowledgements

I would like to start by thanking my supervisor Adrian Lupascu for his assistance and constant mentorship throughout my degree. I am thankful for all that I have learned working with Adrian and appreciate him for pushing me to succeed in my research endeavours.

Also, I would like to thank other members of my SQD group including Jiahao Shi who proposed the system design and performed numerical simulations which gave me the tools I needed to succeed with this project. I thank Xi Dai who was a constant source of advice for writing and theory, as well as Shaun Ren, Lucas Hak, and Jae Jong Oh who were excellent colleagues who helped in the lab with my projects.

Lastly, I would like to thank the QNFCF cleanroom staff for their support and advice when dealing with the fabrication process of my project.

Dedication

This thesis is dedicated to my parents who have always been a great source of encouragement thought my career, and to my lovely fiancée Rachael who is always there to show me love and support when I need it.

Table of Contents

List of Figures

Chapter 1

Introduction

Superconducting circuits are microfabricated quantum devices that make use of superconducting metal films to carry electrical signals and perform operations. Their quantum properties make them uniquely suited to drive the development of emerging technologies and open new directions for experimental research. These circuits have flexible designs that can be implemented to create quantum devices such as magnetometers, photon detectors, and quantum computers that are of particular interest in today's technological landscape. Josephson junctions, a critical element of these instruments, are structures that consist of two superconductors separated by a weak link in order to harness the quantum properties of superconducting electrons. The junctions have unique properties including a non-linear inductance which can be used to generate a two-level system (TLS) that can be applied as qubit.

One such device that employs Josephson junctions is the flux qubit [20]. A flux qubit consist of a loop of superconducting metal that uses these junctions as well as the property of quantized magnetic flux to create a controllable two-level system. Flux qubits are characterized by macroscopic states such as current flowing continuously through its superconducting loop. These states are relatively straightforward to both control and measure. On the other hand, flux qubits do have some drawbacks compared to other quantum devices. Due to these continuous current states, flux qubits are quite sensitive to flux noise generated by ambient magnetic fields, which induce undesired currents and disrupt the

system.

Flux qubits are often coupled to other flux qubits or waveguides for state initialization and exchange of information. Furthermore, it is desirable to be able to tune this coupling during operation of the flux qubit to achieve specific functionality. Developing methods of tuning the interactions and coupler designs for flux qubits has been an ongoing area of research that can open new avenues in quantum computing and fundamental investigations in quantum mechanics.

1.1 Ultra-strong Coupling in Superconducting Circuits

An atom interacting with an electrodynamic field is a fundamental physical process that is formally described as a TLS interacting with bosonic modes. This so called light-matter interaction is well described by the spin-boson model [17]. In nature, these interactions are generally characterized by the fine structure constant ($\sim$1/137) which defines the interaction strength. On the other hand, the coupling strength can be increased in a properly engineered electromagnetic environment where we find that new phenomena such as quantum Rabi oscillations occur and new hybridized descriptions of light and matter are required [7, 15]. The spin-boson model is a useful for describing these interactions across a range of coupling strengths that can be classified into different regimes based on their distinct properties. In the strong coupling regime, the spin-boson model can be simplified using the rotating-wave approximation [14] to make analytic solutions more viable. However, as the strength of interaction increases, the system enters the ultra-strong coupling (USC) regime, where these approximations begin to break down.

Superconducting circuits are one such experimental test bed where we can tune the interaction strength to explore the USC regime of the spin-boson model. With these circuits, the USC regime has been achieved experimentally by coupling artificial atoms initially to an electrodynamic cavity [1, 18] and later to a continuum of light in an open transmission line [8]. However, these previous works only approximate the coupling strength they

achieve by applying models that use the RWA to microwave spectroscopy rather than direct measurement of the dynamics such as the relaxation time. The reason this was not explored further was due to a design limitation: the coupling strength could not be turned off in their setups. In the USC regime, all the interactions take place in the order of a few nanoseconds which makes direct measurement very challenging. A solution for this is to implement a tunable coupler that can enter the USC regime to allow the light-matter interactions to occur, and then decouple the system to freeze the qubit state and enable measurement of the system. This allows for direct observation of the interaction properties in the USC regime. A tunable coupler such as this also has potential in other experiments around quantum computation and relativistic quantum information [24, 27].

1.2 Outline of Thesis

In this thesis, we demonstrate a tunable coupler for controlling the coupling between an open transmission line and a two-level system in the form of a flux qubit. The device, which was fabricated and tested at the University of Waterloo, shows promise as a tool for exploring the USC regime.

In Ch. 2, we introduce relevant topics in the area of coupling within superconducting circuits. We describe the development of flux qubits and their properties as a two-level system. Next, we elaborate on the spin-boson model to characterize the interactions between a bath of photons that can be generated with a transmission line and the artificial atoms that can be created in superconducting circuits. We then discuss coupling regimes in the spin-boson model ranging from weak coupling to USC. Finally, we establish the motivation for the tunable coupler by showing an experimental protocol that can directly measure the dynamics of the USC regime.

In Ch. 3, we present a tunable coupler device for mediating light-matter interactions. The calibration, model fitting, and coupling range are presented for the device. We demonstrate that the coupler is able to effectively turn off the interactions as well as enter the USC regime. This chapter has been prepared for publication.

Chapter 2

Background on Superconducting Circuits and Coupling to Open Waveguides

2.1 Superconducting Circuits

Superconductivity is a quantum phenomenon where certain metals display the remarkable behaviour of having zero resistance at low temperature. As described by Bardeen-Cooper-Schrieffer (BCS) theory [2], below a critical temperature T_c the electrons in superconductors form Cooper pairs, which are able to move without dissipation through the superconductor. The Cooper pairs are described by a wavefunction $\psi = |\psi|e^{i\phi}$ where $|\psi|$ is related to the density of Cooper pairs and ϕ is the phase of the wavefunction through the superconductor. Josephson junctions are devices consisting of two separate superconductors connected by a weak barrier such as an insulator or a non-superconducting metal through which the Cooper pairs can tunnel as shown in Fig. 2.1. The electron pairs passing through the Josephson junctions are specified by the Josephson relations using the phase difference between the two superconductors $\gamma = \phi_1 - \phi_2$. The first relation is the tunneling current

through the junction described by

$$I = I_c \sin\gamma, \tag{2.1}$$

where I_c is the maximum allowed current through the junction without breaking superconductivity, known as the critical current. The second relation describes the voltage across the junction as

$$V = \varphi_0 \frac{\partial \gamma}{\partial t}, \tag{2.2}$$

where $\varphi_0 = \Phi_0/2\pi$ is the reduced flux quantum derived from the flux quantum $\Phi_0 = h/2e$. As a result of the parallel-plate geometry of the junction, there is also a capacitance C that forms at the junction. These relations can also be rearranged to treat the junction like an inductor to find

$$V = L\frac{dI}{dt} \tag{2.3}$$

which gives the inductance

$$L = \frac{\varphi_0}{I_c \cos\gamma}. \tag{2.4}$$

We find that the junction has a non-linear inductance that is dependant on the phase. This non-linear inductance is what makes these junctions uniquely suited to be used as a qubit as we will discuss later.

We can quantize the energy in superconducting circuits and formulate a useful Hamiltonian for systems with Josephson junctions using circuit quantization methods. These follow very similar to canonical quantization which involves transforming kinetic and potential energy of a system along with its classical coordinates into quantum operators characterized by their commutation relations. We have that the electric energy of the junction is stored in the capacitor is

$$T = \frac{1}{2}CV^2 = \frac{1}{2}C\varphi_0^2\dot{\gamma}^2. \tag{2.5}$$

We can determine the potential energy in the junction by considering the the work done with respect to the changing phase. Assuming we have a phase γ_1 at time t_1 and γ_2 at time t_2, we find

$$\Delta E = \int_1^2 IV dt = \int_1^2 Id\Phi = \int_{\gamma_1}^{\gamma_2} I_c \sin\gamma d(\Phi_0 \frac{\gamma}{2\pi}) = -\varphi_0 I_c \Delta \cos\gamma. \tag{2.6}$$

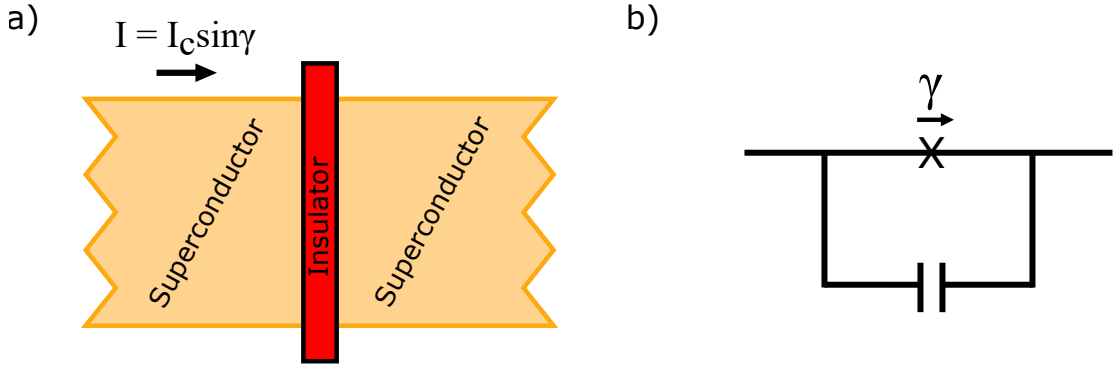

Figure 2.1: (a) Depiction of a Josephson junction. They are formed by separating two superconductors with a weak barrier such as a very thin insulator. A current $I = I_c \sin\gamma$ flows through the junction. (b) A circuit diagram of a Josephson junction. The junction is often just displayed as an X with the capacitance and non-linear inductance inferred.

The change in energy of the junction is independent of the path, so we can thus write this as a potential energy

$$U = -\varphi_0 I_c \cos\gamma. \tag{2.7}$$

We can develop a Lagrangian from these energies that satisfies the Euler-Lagrange equations as

$$\mathscr{L} = T - U = \frac{1}{2} C \varphi_0^2 \dot{\gamma}^2 + \varphi_0 I_c \cos\gamma, \tag{2.8}$$

and find the conjugate momentum p of the coordinate variable γ to be

$$p = \frac{\partial \mathscr{L}}{\partial \dot{\gamma}} = C \varphi_0^2 \dot{\gamma}. \tag{2.9}$$

The Legendre transform can be applied to find the Hamiltonian

$$H = \frac{p^2}{2C\varphi_0^2} - \varphi_0 I_c \cos\gamma. \tag{2.10}$$

As we would with circuit quantization, the classical variables p and γ are converted to quantum operators $\hat{p}$ and $\hat{\gamma}$ with the commutation relationship $[\hat{p}, \hat{\gamma}] = -i\hbar$. We now introduce the energies $E_c = (2e)^2/2C$ as the charging energy and $E_j = \varphi_0 I_c$ as the Josephson energy. These two energies are characteristic parameters that can be easily used to

describe the junction. The final Hamiltonian becomes

$$\hat{H} = \frac{E_c}{\hbar^2}\hat{p}^2 - E_j \cos\hat{\gamma}. \tag{2.11}$$

2.2 Flux qubits

Superconductors also undergo another phenomenon called the Meissner effect, where all magnetic fields are expelled from the superconducting material. A consequence of this property is that through a closed loop of superconducting material the magnetic flux is quantized. As with traditional conductors, current passing through the superconductor induces flux through a loop. When this is combined with any external sources of flux Φ_{ext} we have

$$\Phi = \Phi_{\text{ext}} + LI, \tag{2.12}$$

with L the inductance of the loop. Flux quantization constrains the flux passing through a loop to integer values of a flux quantum Φ_0 as introduced in the previous section.

The flux quantization property can be combined with the Josephson effect to generate flux qubits, which are a type of quantum device that creates a controllable two-level system. One of the early versions of a flux qubit is the RF-SQUID, a large superconducting loop interrupted by a a single junction as seen in Fig. 2.2(a). There is a phase relationship that arises from the Josephson junction and the flux through the superconducting loop. This is a direct result of the inherent wavefunction of the superconductor, where the phase must be periodic and continuous. For an RF-SQUID, the phase around the loop of superconductor obeys the condition

$$\gamma = -2\pi\frac{\Phi}{\Phi_0}, \tag{2.13}$$

which then can be expanded using Eq. (2.12) to get

$$\gamma = -2\pi f - \frac{L_{\text{sq}} I_{\text{sq}}}{\varphi_0}, \tag{2.14}$$

where $f = \Phi_{\text{ext}}/\Phi_0$ is the external dimensionless flux passing through the loop, $L_{\text{sq}} = L_g + L_k$ the inductance of the RF-SQUID, with L_g the self inductance of the loop and L_k

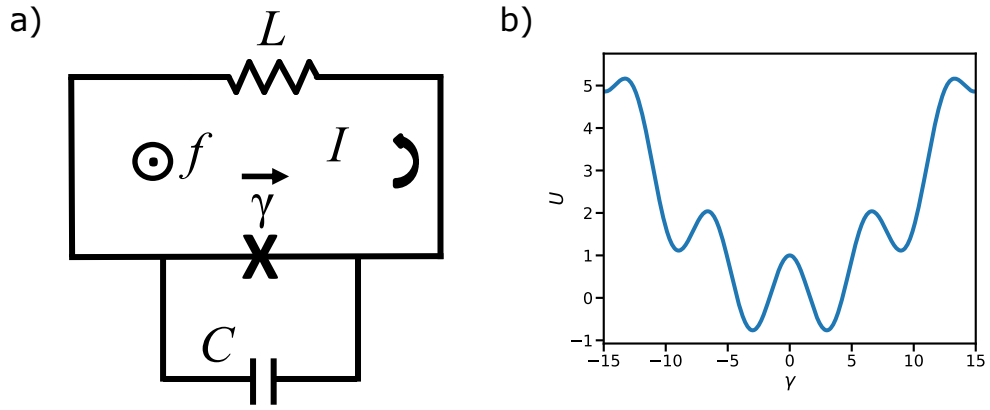

Figure 2.2: (a) Circuit diagram for an RF-SQUID: a superconducting loop with a single Josephson junction γ. The junction has capacitance C, the current circulating the loop is I, and the geometric inductance of the loop is L. The flux through the loop is quantized as $f = \Phi_{ext}/\Phi_0$. (b) Potential energy U vs phase γ for the RF-SQUID at $f = \frac{1}{2}$ forming a double well potential.

the kinetic inductance arising from the motion of Cooper pairs, and I_{sq} is the circulating current. For the loop we also have the current

$$I_{\text{sq}} = I_c \sin\gamma + \varphi_0 C\ddot{\gamma}. \tag{2.15}$$

We can proceed with the same steps beginning at Eq. (2.5) to derive the Hamiltonian for the RF-SQUID. We begin with the kinetic energy T and potential energy U of the system, then introduce the Lagrangian and the conjugate momentum, and finally perform the Legendre transform to recover the Hamiltonian. We have the same kinetic energy

$$T = \frac{1}{2} C\varphi_0^2\dot{\gamma}^2, \tag{2.16}$$

as before. We determine the potential energy by accounting for both the energy of the junction described in Eq. (2.7) and the energy stored in the self-inductance of the loop $U = \frac{1}{2}L_{sq}I_{sq}^2$, and substitute Eq. (2.14) into the system to produce

$$U = -\varphi_0 I_c \cos\gamma + \frac{\varphi_0^2}{2L}(\gamma + 2\pi f)^2. \tag{2.17}$$

With this we find the Hamiltonian as

$$H = \frac{E_c}{\hbar^2} p^2 - E_J \cos\gamma + \frac{\varphi_0^2}{2L}(\gamma + 2\pi f)^2. \tag{2.18}$$

Due to the quadratic second term, the RF-SQUID has a deep potential minima when the screening parameter $\beta = LI_c/\varphi_0$ is large. When we set $f = \frac{1}{2} + n$ with n an integer, a double well potential forms and the SQUID has degenerate lowest-energy states as seen in Fig. 2.2(b). This result shows that the non-linear inductance of the Josephson junction can be used to generate anharmonicity in the system to transform the RF-SQUID into a two-level-system (TLS). Therefore, it is feasible to use RF-SQUID as a qubit. The drawback of the RF-SQUID is that in order to create appropriate potential wells for the system, the geometric inductance and hence the size of the loop must be large. This large size make the any device made using an RF-SQUID highly sensitive to flux noise which leads to decoherence in the generated qubit.

A solution to this issue was proposed in the form of the persistent current qubit (PCQ) which instead utilizes three Josephson junctions in loop as seen in Fig. 2.3(a). The junctions γ_1 and γ_3 are identical with Josephson energy E_J, while γ_2 is called the α_{pcq} junction (distinct from the coupling strength α) and is made smaller with a Josephson energy $\alpha_{pcq}E_J$ with $\alpha_{pcq} < 1$. This new design has a much smaller loop size so the self-inductance can be neglected in the updated phase relationship. This relation becomes

$$\gamma_1 + \gamma_2 + \gamma_3 = -2\pi f. \tag{2.19}$$

The condition in Eq. (2.19) can be used to constrain the Lagrangian to retain only two degrees of freedom γ_1 and γ_3. With this constraint in place, the Hamiltonian becomes

$$H = \frac{\hbar^2}{2} E_c \boldsymbol{p} \tilde{C}^{-1} \boldsymbol{p}^T + U(\gamma_1, \gamma_3), \tag{2.20}$$

where $\boldsymbol{p} = (p_1, p_3)$ is the set of conjugate momenta to the phases, $\tilde{C}$ is the capacitance matrix given as

$$\tilde{C} = \begin{bmatrix} 1 + \alpha_{pcq} & \alpha_{pcq} \\ \alpha_{pcq} & 1 + \alpha_{pcq} \end{bmatrix}, \tag{2.21}$$

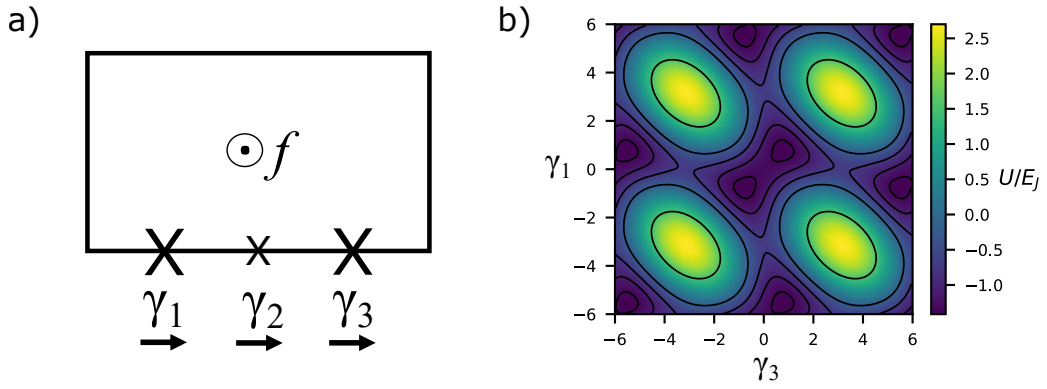

Figure 2.3: (a) The circuit diagram for a persistent current qubit (PCQ) with three Josephson junctions γ_i. The flux through the loop is quantized as $f = \Phi_{\text{ext}}/\Phi_0$. (b) Potential energy vs phase for the PCQ with a double well potential in the center. The two wells correspond to different states of current flowing in opposite directions.

and $U(\gamma_1, \gamma_3)$ is the potential energy

$$U(\gamma_1, \gamma_3) = -E_J(\cos\gamma_1 + \alpha_{pcq}\cos(2\pi f + \gamma_1 + \gamma_3) + \cos\gamma_3). \tag{2.22}$$

The PCQ is named as such because this design results in a persisting current circulating through the superconducting loop. Just like with the RF-SQUID, there is a resulting double-well potential in the PCQ that is now periodic in γ_1 and γ_3 as illustrated in Fig. 2.3(b). The two different wells correspond to macroscopic states when the current is flowing in opposite directions, either clockwise or anti-clockwise. These different currents have well defined phases and are referred to as flux states. When $f = \frac{1}{2}$, the well becomes symmetric, making the energy levels degenerate and allowing for tunnelling between the two flux states. Neglecting higher energy levels and treating this as a two level system, the Hamiltonian can be written in this flux basis as

$$H = -\frac{\hbar\Delta}{2}\sigma_x - \frac{\hbar\epsilon}{2}\sigma_z, \tag{2.23}$$

with $\hbar\Delta$ is the energy for the minimum TLS gap, $\hbar\epsilon$ is the energy difference between the two potential wells, and σ_x, σ_z are the Pauli operators. We have that

$$\epsilon = \frac{2I_p\Phi_0}{\hbar}(f - \frac{1}{2}), \tag{2.24}$$

where I_p is the persistent current in the loop. When the external flux is $f = \frac{1}{2}$ the qubit is positioned at what is known as the symmetry point where the energy difference is at a minimum Δ. In general for an arbitrary flux bias f, the frequency for the energy gap of the PCQ is

$$\omega_{10} = \sqrt{\Delta^2 + \epsilon^2}. \tag{2.25}$$

In the energy eigenbasis, the Hamiltonian is written as

$$H = -\frac{\hbar\omega_{10}}{2}\sigma_z. \tag{2.26}$$

2.3 Ultra-Strong Coupling in Superconducting Circuits

2.3.1 Spin-Boson Model

The spin-boson model [17] is a useful model for describing solid state systems, chemical reactions, and most notably for our purposes, the interactions between light and matter. The model relates spins, such as a two-level system, to bosons, such as a bath of photons under various conditions. The photon bath is represented as a set of harmonic oscillators and can be treated as a continuous or discrete set depending on the system involved. These interactions have a coupling value α which gauges the strength of the interactions and has several implications for the behaviour of the system [15]. In nature, the electromagnetic coupling strength between elementary charged particles is $\sim$1/137 and is known as the fine structure constant. This relatively small coupling strength emerges from a perturbative treatment of quantum electrodynamics and is used to describe processes such as photon absorption or emission by a charged particle. However, Purcell discovered in 1946 that light-matter interactions can be controlled to suppress or intensify the coupling in different electromagnetic environments [25]. For instance the interaction strength can be altered using an photonic resonator coupled to an artificial atom. For large enough values of coupling strength ($\alpha \sim 0.1$), the system enters what is known as the ultra-strong coupling (USC) regime of light-matter interactions.

For a two-level system coupled to a bosonic bath, the Hamiltonian is written as

$$\hat{H}_{\mathrm{SB}} = \hat{H}_0 + \hat{H}_{\mathrm{int}} = \frac{\hbar\Delta}{2}\hat{\sigma}_z + \sum_k \hbar\omega_k \hat{a}_k^\dagger \hat{a}_k + \hat{\sigma}_x \sum_k g_k(\hat{a}_k + \hat{a}_k^\dagger), \tag{2.27}$$

where $\hat{H}_0$ is the first two terms of the Hamiltonian corresponding to the two-level system using Eq. (2.26) and the bosonic bath respectively, and $\hat{H}_{int}$ corresponds to the third term (the interaction term). The frequency Δ corresponds to the two-level system splitting, σ_z and σ_x are the Pauli operators, $\theta = \arctan(\frac{\Delta}{\epsilon})$ is determined by the qubit bias, and ω_k, $\hat{a}_k^\dagger$, $\hat{a}_k$ are frequency, creation, and annihilation of the k^{th} mode of the harmonic oscillator. The term g_k represents the coupling strength between the TLS and the bath. The values for g_k can be described by a spectral density function and in an ohmic environment can be simplified as [21]

$$J(\omega) = \frac{2\pi}{\hbar^2}\sum_k g_k^2 \delta(\omega - \omega_k) = \pi\omega\alpha, \tag{2.28}$$

where α is a dimensionless constant used to describe the coupling of the system. Using the Born-Markov approximation [32], this interaction term can be related to the level splitting Δ of the system through the relaxation rate Γ_{01} of the TLS to the bath with the relation

$$\alpha = \Gamma_{01}/\pi\Delta. \tag{2.29}$$

The coupling strength given by these equations has strong implications for the system as a whole. There are four distinct regimes of light-matter interaction that result from this model: weak coupling, strong coupling, ultra-strong coupling (USC), and non-perturbative USC [15]. The weak coupling regime is characterized by coupling g that is smaller than the losses of the system so the energy is dissipated before interactions can occur. In the strong coupling regime, light-matter interactions take place but qubit relaxation rate is much smaller than the transition frequency $\Gamma/\Delta \ll 1$. Here the coupling is strong enough for quantum Rabi oscillations to occur. The dynamics of this regime are often described using the rotating wave approximation (RWA) which assumes that, at the symmetry point where we only have transverse coupling, the fast oscillations of counter-rotating terms in the interaction Hamiltonian will average out and are discarded. What is left is called the Jaynes-Cummings Hamiltonian given by [14]

$$H_{JC} = \frac{\hbar\Delta}{2}\sigma_z + \hbar\omega a_k^\dagger a_k + g(\sigma_+ a + \sigma_- a^\dagger), \tag{2.30}$$

where $\sigma_+ = |e\rangle\langle g|$ and $\sigma_- = |g\rangle\langle e|$ are ladder operators of the qubit. This formulation describes coherent interaction transferring conserved excitations between the TLS and the bath.

The interactions enter the USC regime as $\Gamma/\Delta \gtrsim 0.1$. In this regime, the counter-rotating terms that were discarded previously in the Jaynes-Cummings Hamiltonian become relevant and the previous approximation is not applicable. With this simplification missing, analyzing the dynamics of the system becomes far more challenging. We must begin treating light and matter in terms of hybrid states instead of distinct entities [7]. In the USC regime, the Born-Markov approximation continues to hold. Beyond this however, as the relaxation rate starts to exceed the qubit gap $\Gamma/\Delta \gtrsim \frac{\pi}{2}$ the system enters the non-perturbative USC regime. Here, the Born-Markov approximation no longer holds and the relationship of Eq. (2.29) becomes a lower bound for the system coupling α. In this regime, higher order perturbative processes begin to dominate the interaction and the system is characterized by photons dressing the atoms even in their ground state.

2.3.2 Flux Qubit Coupled to a Waveguide

One way to explore the interactions described and the different coupling regimes by the spin-boson model is through specially designed superconducting circuits. We can generate a bosonic bath in the form of a waveguide and an artificial atom in the form of a flux qubit to probe their interactions. Based on the formulations of Sec. 2.2, we see that PCQs biased at their symmetry point already have a Hamiltonian of the form seen in the spin-boson model. In addition to this, we will now show how a coupled waveguide is introduced into this system.

Transmission lines (TL) are a type of electrical component such as coaxial cables that are used to conduct electromagnetic signals and transfer energy. Ideal lines are characterized by their characteristic impedance $Z_0 = \sqrt{l_0/c_0}$ using the inductance and capacitance per unit length, and the transmission of voltage and current through the line are described by the well-known telegrapher's equations [11]. Superconducting circuits often make use of co-planar waveguides (CPW), which are a form of transmission line consisting of a center conductor separated from a ground plane by a gap of dielectric material as seen in Fig. 2.4.

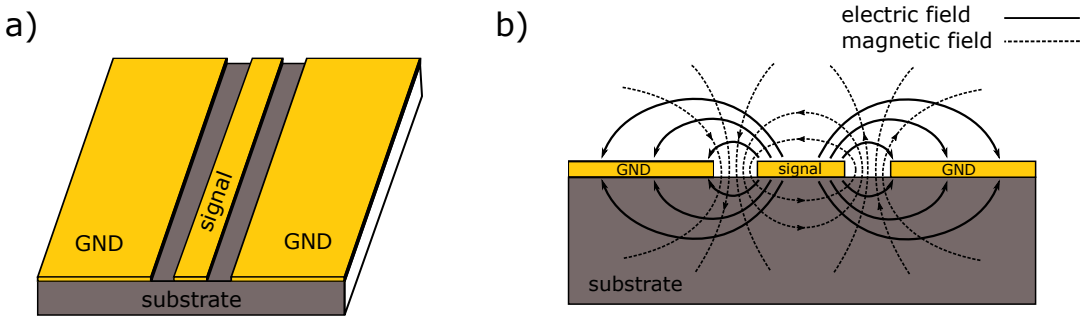

Figure 2.4: A co-planar waveguide (CPW) which is often used in superconducting devices. (a) The general structure of a CPW with the signal line separated from the ground planes on the dielectric. Power is transferred in the direction of current flowing on the signal line. (b) A cross section of the CPW with electric and magnetic field lines.

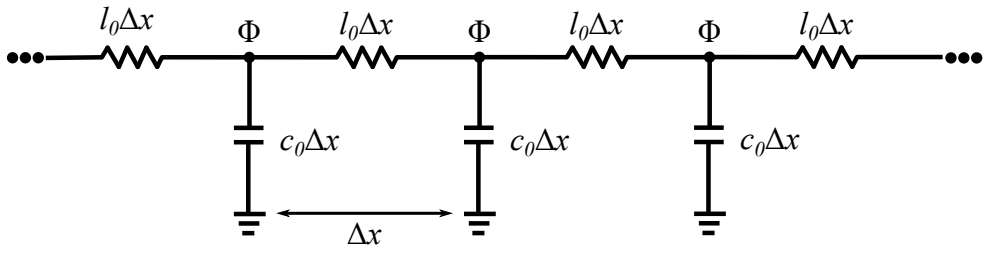

Figure 2.5: A transmission line treated as an infinite series of LC resonators for quantization.

CPWs are quite simple to manufacture, and, like all transmission lines, efficiently carry power down the signal line through its interacting electric and magnetic fields.

Like other circuit elements, transmission lines can be quantized. The infinitely long (open) transmission line is treated as a series of LC circuits as shown in Fig. 2.5. The Hamiltonian is determined by starting with the system charging energy stored in the capacitance and the magnetic energy stored in the inductance of each point. The result is then

$$H = \int_{-\infty}^{\infty} dx \left(\frac{q(x,t)^2}{2c_0} + \frac{(\partial_x \Phi(x,t))^2}{2l_0} \right), \tag{2.31}$$

where $q(x,t)$ is the charge density and $\Phi(x,t)$ is the magnetic flux at a given position x and time t. The Hamiltonian can be transformed in terms of the charge density operator $\hat{q}(x,t)$ and its canonical momentum $\hat{\Phi}(x,t)$ which follow the typical commutation relation $[\hat{q}(x,t), \hat{\Phi}(x',t)] = -i\hbar\delta(x-x')$. Using these, the transmission line is quantized as

$$\hat{H} = \sum_k \hbar\omega_k (\hat{a}_k^\dagger \hat{a}_k + \frac{1}{2}), \tag{2.32}$$

where ω_k is the frequency corresponding to mode k, $\hat{a}_k^\dagger$ and $\hat{a}_k$ are the ladder operators with relationships to the charge and flux operators as

$$\hat{q}(x,t) = i\frac{c_0}{\sqrt{2L}} \sum_k \sqrt{\hbar\omega_k} \left[\hat{a}_k e^{i(kx-\omega_k t)} - \hat{a}_k^\dagger e^{-i(kx-\omega_k t)} \right], \tag{2.33}$$

$$\hat{\Phi}(x,t) = \frac{1}{\sqrt{2Lc_0}} \sum_k \sqrt{\frac{\hbar}{\omega_k}} \left[\hat{a}_k e^{i(kx-\omega_k t)} + \hat{a}_k^\dagger e^{-i(kx-\omega_k t)} \right], \tag{2.34}$$

with L the length of the transmission line. The transmission line is now of the form of a quantum harmonic oscillator similar to the bosonic bath in the spin-boson model. One can easily convert the charge operator to voltage by dividing by c_0 for measurement and control purposes.

Next we consider the coupling between this transmission line and flux qubit. This result can be obtained by looking at the specific case for a four junction PCQ galvanically connected to an open transmission line as illustrated by Fig. 2.6. The transmission line is formed of an infinite series of LC resonators as before and the PCQ is considered a

lumped element inserted into the series at $x = 0$. With this setup, the time-independent Hamiltonian is solved as [21]

$$H = \int_{-\infty}^{\infty} dx \left(\frac{q(x)^2}{2c_0} + \frac{(\partial_x \Phi(x))^2}{2l_0} + \delta(x)\frac{1}{l_0}\partial_x \Phi(x)\varphi_0\gamma_4 \right) + \frac{1}{2l_0\Delta x}(\varphi_0\gamma_4)^2 + H_{qb}, \quad (2.35)$$

with $\delta(x)$ the Dirac delta function and H_{qb} is the qubit Hamiltonian described by Eq. (2.26). We see that this has the same form as a qubit plus Eq. (2.31) with two additional terms.

The fourth term, which can be seen outside the integral, is a renormalization to the qubit term that causes a shift in the potential. Replacing $l_0\Delta x = Z_0/\omega$ and subbing in a general value of $Z_0 = 50\ \Omega$, we obtain the qubit renormalization as

$$H_{\text{renorm}} \sim \hbar\omega \frac{\hbar}{16 Z_0 e^2}\gamma_4^2 \sim 5.2\hbar\omega\gamma_4^2, \quad (2.36)$$

with $\omega \sim 2\pi(1-8)\ GHz$. This value is much smaller than typical potentials for flux qubits of

$$E_j/\hbar = 250 - 800\ GHz, \quad (2.37)$$

and can thus be neglected in the Hamiltonian.

The third term which, falls inside the integral, arises from the shared junction γ_4 and represents the interaction between the qubit and the transmission line H_{int}. After integration we obtain

$$H_{\text{int}} = \frac{1}{l_0}\partial_x \Phi(0)\varphi_0\gamma_4. \quad (2.38)$$

The interaction term can be used to estimate the coupling strength of the the system. If we substitute the time-independent form of $\hat{\Phi}$ operator from Eq. (2.34) into the interaction term the result is

$$H_{\text{int}} = \frac{1}{l_0}\varphi_0\gamma_4 \sum_k \sqrt{\frac{\hbar}{2Lc_0\omega_k}} k \left(\hat{a}_k + \hat{a}_k\right). \quad (2.39)$$

Further, assuming the system is near the symmetry point ($\theta \sim \frac{\pi}{2}$), the interaction term in Eq. (2.27) from the spin-boson model was found to be

$$H_{\text{int}} = \hat{\sigma}_x \sum_k g_k(\hat{a}_k + \hat{a}_k^\dagger). \quad (2.40)$$

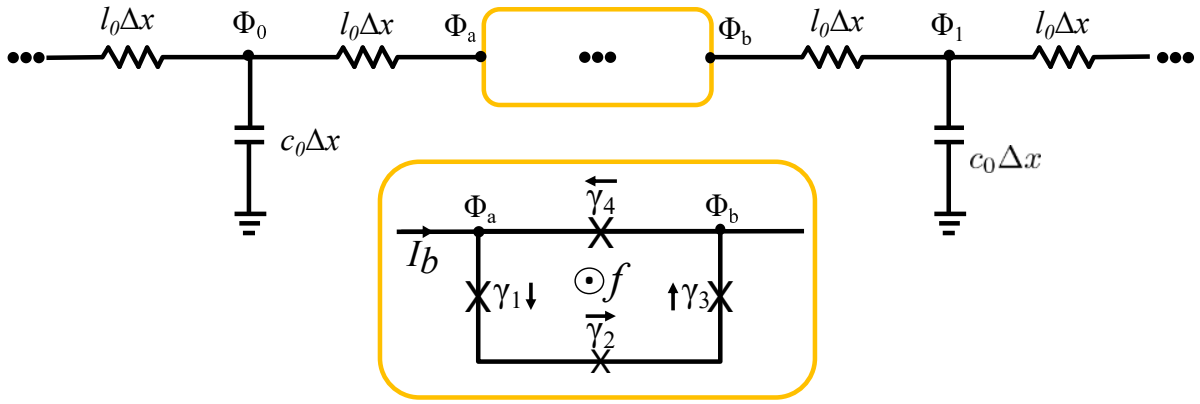

Figure 2.6: A quantized transmission line where additional lumped element components can be inserted into the yellow box. A lumped element PCQ is depicted below this that can be coupled to the transmission line.

By comparison of these two equations and applying $k = \frac{\omega_k}{c}$, we see that the coupling strength for mode k is

$$g_k = \frac{1}{l_0}\varphi_0|\gamma_{4_{10}}|\sqrt{\frac{\hbar\omega_k}{2Lc_0c^2}}, \tag{2.41}$$

with $\gamma_{4_{10}} = \langle 1|\gamma_4|0\rangle$ the matrix element of the phase operator and $c = \frac{1}{\sqrt{l_0c_0}}$ the speed of light through the transmission line. It is clear that this interaction strength stems from both the qubit and the transmission line properties, with strong dependence on the shared junction.

2.3.3 Previous Coupler Designs

One important challenge that arises when coupling a flux qubit to a waveguide is being able to mediate this coupling and control how strongly the two systems interact. In order to characterize the dynamics of the different regimes in the spin-boson model, we must control the coupling constant α through some means so that it can be analyzed over a range of values. Furthermore, as we will discuss in the next section, mediating the coupling is necessary for such experiments like measuring relaxation rate which occurs too quickly to measure directly in the USC regime.

In this section we will look at several tunable coupler designs for flux qubits that have been previously presented in literature. First, rather than looking at a flux qubit coupled directly to a waveguide, to gain some additional intuition and prior context on couplers, we will look at designs for tunable couplers between two flux qubits. A pair of early designs used either an auxiliary RF- or DC-SQUID to mediate the interactions between the flux qubits [4, 23]. The circuit diagram for these couplers can be seen in Fig. 2.7 (a) and (b) where there are two PCQs separated by an RF-SQUID and DC-SQUID respectively. We will now look a little closer at the case of the RF-SQUID where the coupling arises from classical mutual inductance. The effective mutual inductance between the two qubits is

$$M_{\text{eff}} = \frac{M_1 M_2}{L_{\text{sq}}}, \tag{2.42}$$

where M_i is the coupling from each qubit to the mediating SQUID and $1/L_{\text{sq}}$ is the susceptibility of the SQUID. We also have

$$\frac{1}{L_{\text{sq}}} = \frac{dI_{\text{sq}}}{d\Phi_{\text{ext}}}. \tag{2.43}$$

Putting these together with the standard inductance relation returns

$$\Phi_2 = M_{\text{eff}} I_{p_1} = \frac{M_1 M_2}{L_{\text{sq}}} I_{p_1} = M_1 M_2 \frac{dI_{\text{sq}}}{d\Phi_{\text{ext}}} I_{p_1}, \tag{2.44}$$

with Φ_2 the flux in the second qubit and I_{p_1} the persistent current through the first qubit. This demonstrates a relationship between the state of the two qubits. The coupling strength of this interaction is

$$g = M_{\text{eff}} I_{p_1} I_{p_2}. \tag{2.45}$$

This shows that the coupling strength between the two qubits can be mediated by changing $dI_{\text{sq}}/d\Phi_{\text{ext}}$. Through Eq. (2.15) and Eq. (2.14), this value can be tuned to establish some control over the coupling strength.

This concept for using a SQUID to mediate coupling can also be used to couple to a transmission line. A diagram showing this method of coupling is shown in Fig. 2.7(c). A different variation of this coupler was implemented in Ref. [8] where coupling between a flux qubit and a transmission line was demonstrated up to the non-perturbative USC

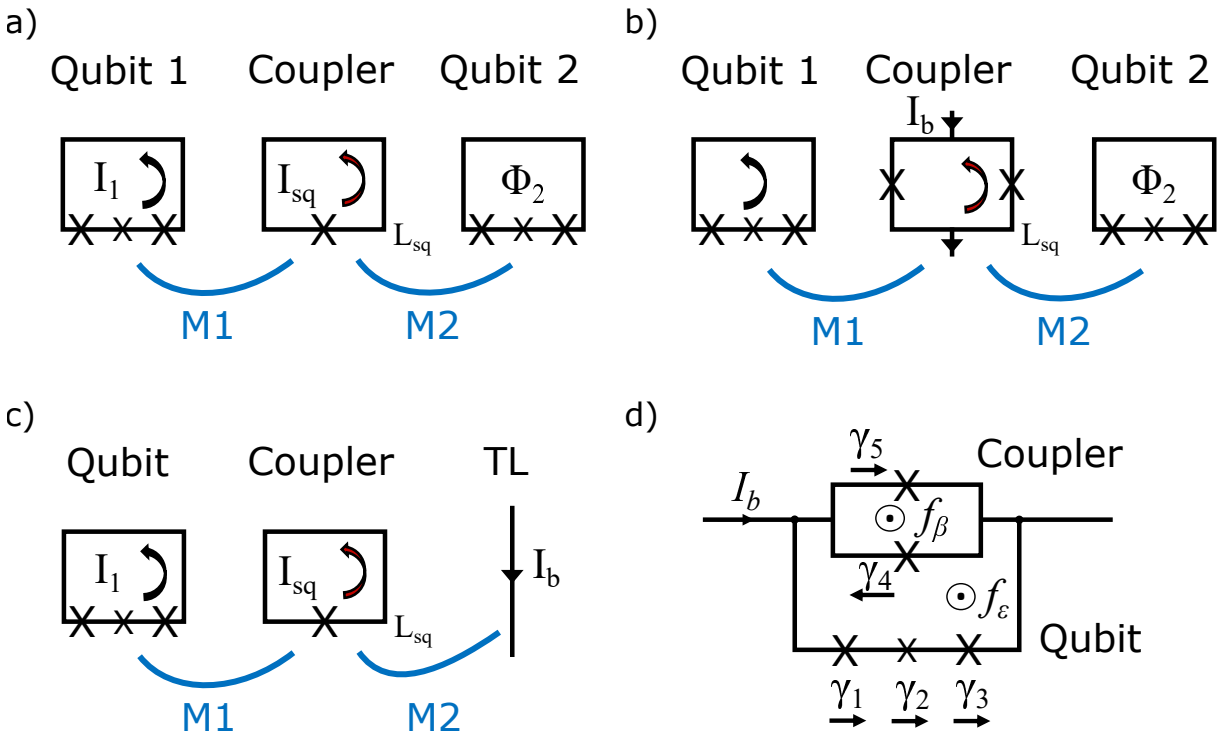

Figure 2.7: Various tunable coupler designs from previous work. The couplers generally work by generating a tunable mutual inductance between the current in qubit 1 and the target component. (a) Two flux qubits mediated by an RF-SQUID. (b) Two flux qubits mediated by an DC-SQUID. (c) A flux qubit coupled to a transmission line with an RF-SQUID (d) A flux qubit coupled to a transmission line with a galvanically coupled RF-SQUID.

regime ($\alpha \gtrsim 1/2$). A circuit diagram for this design can be seen in Fig. 2.7(d) where a flux qubit is galvanically connected to a transmission line. The coupling can be approximated by MI_p with M the mutual inductance between the qubit and the transmission line and I_p the persistent current of the qubit. The mutual inductance is dominated by the non-linear Josephson inductance L_J of the shared junction as discussed in Sec. 2.3.2. When the current flowing through the junction is much smaller than its critical current ($I \ll I_c$), the Josephson inductance behaves as a linear inductor with $L_J \approx \varphi_0/I_c$.

There are four junctions γ_1-γ_4 in the main qubit loop with γ_4 replaced by an RF-SQUID. This SQUID acts as a tuning device by acting effectively as a junction with critical current that varies between $|I_{c4}+I_{c5}|$ - $|I_{c4}-I_{c5}|$. Thus there is a range from a minimum inductance

$$L_{J,\min} = \frac{\varphi_0}{|I_{c4} + I_{c5}|}, \tag{2.46}$$

to the maximum inductance

$$L_{J,\max} = \frac{\varphi_0}{|I_{c4} - I_{c5}|}, \tag{2.47}$$

which corresponds to the achievable range of coupling. The device is operated by changing the fluxes $f_\epsilon = \Phi_\epsilon/\Phi_0$ and $f_\beta = \Phi_\beta/\Phi_0$ through the two superconducting loops. The flux in the coupling SQUID f_β mediates the coupling to the transmission line while f_ϵ is used to control the PCQ in the system. The design is capable of achieving very large coupling; however the minimum inductance is not small enough to adequately decouple the flux qubit from the TL. The decoupling can be improved with larger junctions, but these are not feasible for standard fabrication techniques.

2.4 Proposal for USC Time-domain Testing

The USC regime of light-matter interactions is an area of research that still has much to be explored including the time-domain dynamics of this regime. As discussed in Sec. 2.3.1, the rotating-wave approximation for the spin-boson model breaks down in the USC regime and the Jaynes-Cummings Hamiltonian can no longer be applied to simplify the system. As a result, analytic models of the interactions only produce estimates of the coupling

strength and the time-domain dynamics. In this section, we propose an experiment for directly measuring the time-domain dynamics.

In quantum computation, one of the most important characteristics of a qubit is its relaxation time T_1 which describes the time taken for a qubit to transition from its excited state to the ground state. This relaxation of a TLS to a coupled waveguide demonstrates the dynamics of the system and can be used as a measurement of the coupling strength. In contrast to analytic models that use the RWA, a T_1 measurement will be a direct measurement of the interactions without involving approximations. However, the light-matter interactions that occur in the USC regime, including relaxation, take place over very short time scales at a rate comparable with the frequency of the photons being exchanged. For microwaves in the GHz range, this time scale is on the order only a few nanoseconds. To work around this constraint, a system with tunable coupling must be able to effectively decouple the TLS from the transmission line in order to freeze the qubit state and prevent further relaxation.

The tunable coupler we propose for performing this experiment is a two-loop flux qubit coupled to a transmission line where the flux $f_\beta = \Phi_{\beta,\text{ext}}/\Phi_0$ controls the coupling strength and flux $f_\epsilon = \Phi_{\epsilon,\text{ext}}/\Phi_0$ controls the two-level system. The two-level system is a PCQ that must to be biased at its symmetry point where a symmetric double well potential forms. There is also readout resonator that is inductively coupled to the PCQ. We introduce a protocol to measure the relaxation rate as shown in Fig. 2.8. The protocol is performed as follows:

- Step 1: The flux biases f_β and f_ϵ are set to a symmetry point of the qubit with weak coupling. The qubit starts in its ground state before being excited with a π pulse through f_ϵ.
- Step 2: The flux biases are fast tuned to a new symmetry point that has stronger coupling. This process is done faster than the qubit evolution or relaxation to ensure the state is unchanged during the process.
- Step 3: The qubit remains at this symmetry point for a delay time d_t, during which the qubit relaxes toward its ground state through the interactions that have a strength

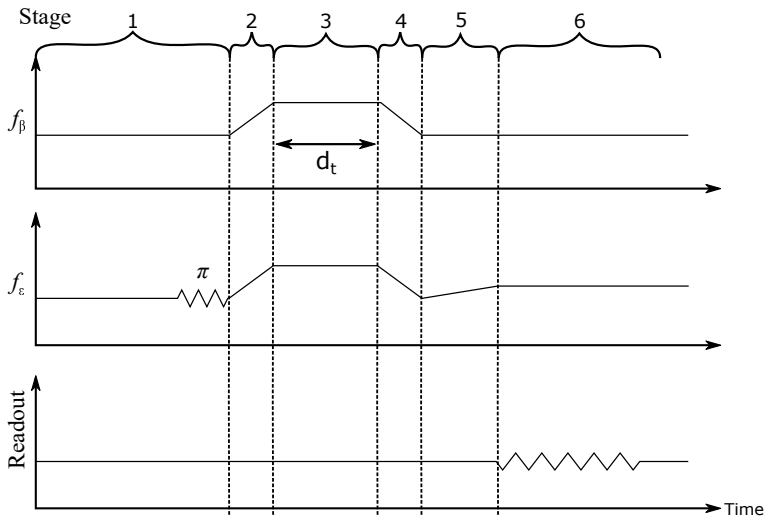

Figure 2.8: Diagram of the experimental protocol for measuring the relaxation rate, T_1, of the qubit when coupled to the transmission line. This procedure as described in the text will allow characterization of the very short timescale interactions of the USC regime.

α.

- Step 4: The flux biases are fast tuned back to the weak coupling point of step 1 to switch the coupling off and stop the qubit from further relaxation.
- Step 5: The qubit is adiabatically tuned to an off-symmetry point where the energy states become flux-like state for readout. This process should be done slower than the evolution of the qubit Hamiltonian at the qubit frequency, but faster than the relaxation rate to keep the state frozen.
- Step 6: Readout is performed with pulses sent to a feedline that is coupled to the readout resonator.

This procedure is repeated with variable time delays and coupling strengths to characterize the relaxation rate in USC regime. In addition, other tests along the same vein can be done to further explore the USC regime. We can measure qubit dephasing using a Ramsey experiment protocol, and we can measure the tunnelling frequency of flux states[28].

Chapter 3

Tunable Coupler for Mediating Interactions of a Two-Level System to a Waveguide from Weak to Ultra-Strong Coupling

Ultra-strongly coupled light-matter interactions [15, 17] enabled through specially designed electromagnetic environments are exciting for their emerging applications in the fundamental study of the spin-boson model [28], non-linear optics [16], and relativistic quantum information processing [26, 27, 24, 30]. Recent advancements in superconducting circuit design allow us to exceed the natural limit of light-matter coupling to explore the ultra-strong coupling (USC) regime of these interactions [29, 3, 8]. Often, these designs are constrained to a single coupling strength, which limits their experimental capability. We present a device capable of mediating the light-matter coupling between a two-level system (TLS) and a waveguide achieving a large range of coupling. Akin to the general spin-boson model of light-matter interactions, the coupling strength between a TLS and a waveguide can be described as [8]

$$\alpha = \frac{\Gamma_{01}}{\pi\Delta}, \tag{3.1}$$

where Γ_{01} is the relaxation rate and Δ is the energy level splitting of the TLS. We demonstrate a coupling strength α from 2.4×10^{-4} to 1.2×10^{-1} between a TLS and waveguide. This enables exploring the interaction over a span of several qualitatively distinct regimes including the USC regime ($\alpha \sim 0.1$) where the relaxation rate becomes comparable to the splitting frequency and the rotating wave approximation (RWA) breaks down [14, 21]. The device is designed to use fast-switchable coupling to perform direct measurements of these short time scale interactions.

The tunable coupler we introduce in this section couples a TLS implemented as a persistent current qubit (PCQ) [20] to an open transmission line (TL). Unlike previous work that explored the USC regime using flux qubits [8], our design not only enables the USC regime, but also has the distinct advantage that it can effectively decouple the TLS and the TL. This is done by using a second PCQ as the coupler. The circuit diagram shown in Fig. 3.1(a) illustrates a TL with two superconducting loops and six junctions γ_i. The first loop a is 4-junction PCQ that forms the qubit loop and has an external flux bias $f_\epsilon = \Phi_{\epsilon,\text{ext}}/\Phi_0$ with $\Phi_0 = h/2e$ the magnetic flux quantum. The second loop is a 3-junction PCQ that forms the coupling loop and is biased by a flux $f_\beta = \Phi_{\beta,\text{ext}}/\Phi_0$. Further details on the qubit circuit and it's use with the circuit model are discussed in Appendix A. For the TLS, we have a Hamiltonian of the form

$$H = -\frac{\hbar\Delta}{2}\sigma_x - \frac{\hbar\epsilon}{2}\sigma_z, \tag{3.2}$$

where Δ is the minimum gap, σ_x and σ_z are the Pauli matrices, and $\epsilon = \frac{2I_p\Phi_0}{\hbar}(f_\epsilon - f_{\epsilon,\text{sym}})$ with and I_p the persistent current in this loop. The flux $f_{\epsilon,\text{sym}}$ is the bias through the ϵ-loop that produces the minimum qubit gap known as the symmetry point. For an arbitrary flux biasing, the Hamiltonian results in a gap frequency of

$$\omega_{10} = \sqrt{\Delta^2 + \epsilon^2}, \tag{3.3}$$

which is equal to Δ at the symmetry point. It is necessary to operate the qubit at its symmetry point to form a symmetric double well potential characteristic of PCQs which ensures that the light-matter coupling is transverse.

The coupler design relies on the effective quantum inductance of the coupling loop to mediate the light-matter interaction. Qualitatively, the interaction between the qubit loop

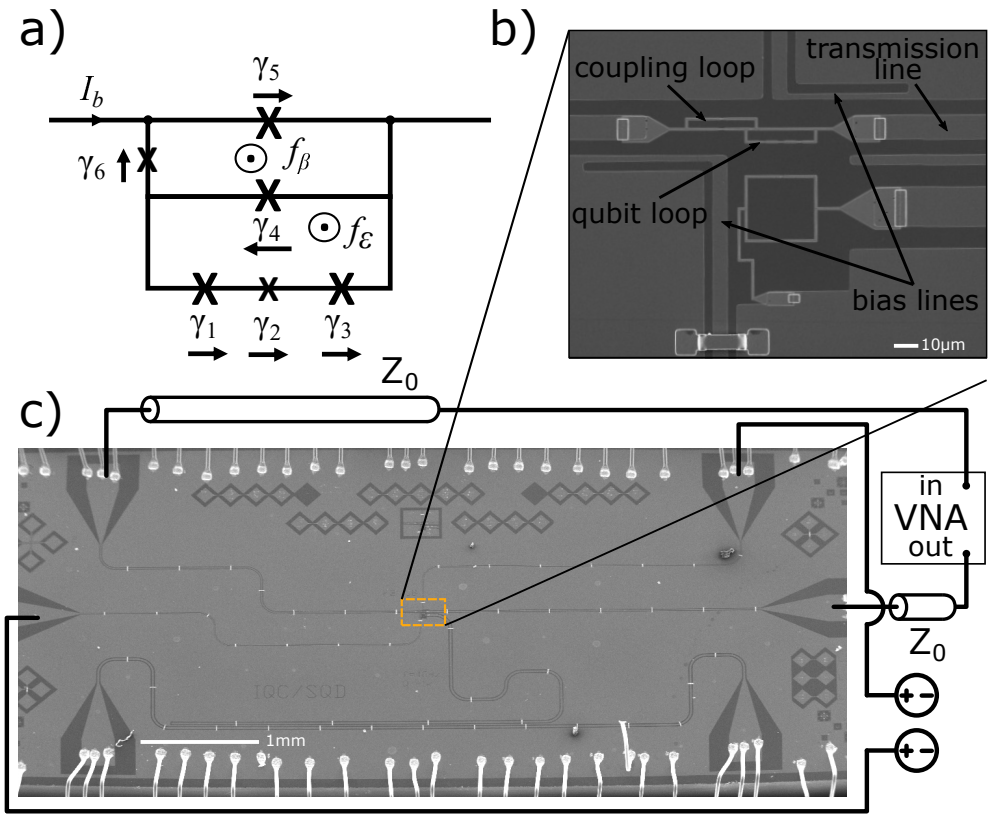

Figure 3.1: (a) The circuit diagram including the qubit loop, the coupling loop, and the transmission line in the form of a current I_b. The fluxes f_β and f_ϵ are external biases that pass through the coupling loop and qubit loop respectively. (b) An SEM image of the tunable coupler device. Note that the layout of the bias lines shown use a single arm $'L'$ shape while the tested device was a variation that uses a two arm $'T'$ shape. (c) An SEM image of the full device. The ends of the transmission line are connected to a VNA for measurement and the bias lines are connected to external voltage sources.

and the TL can be considered analogous to the interaction between two flux qubits [4, 31]. They interact through an effective mutual inductance M_{eff} controlled by the coupling loop. We have that $M_{\text{eff}} = M_{\text{tls}} M_{\text{tl}} / L_\beta$ where M_{tls} (M_{tl}) is the mutual inductance between the coupling loop and TLS (TL) and $1/L_\beta$ is the susceptibility of the coupling loop. We have $1/L_\beta = \frac{1}{\Phi_0} \partial I_g / \partial f_\beta$ where I_g is its ground state current, so the coupling loop was optimized for a large range of $1/L_\beta$ that can be tuned by changing f_β. Further, M_{tls} and M_{tl} are predominantly supplied by the inductance of the shared junctions γ_4 and γ_5 respectively [21, 8].

A scanning electron microscope (SEM) image of the device shown in Fig. 3.1(b) depicts the qubit loop, the coupling loop, and the TL. The flux is controlled via two bias lines that are used to independently bias each loop as will be shown in the following discussions. The design includes a DC-SQUID that is inductively coupled to the qubit loop that can be used for readout of the TLS, though it was not used for this test. The full device and the experimental setup are displayed in Fig. 3.1(c) where it is shown that the bias lines are each driven with an external voltage source and the signal through the TL is measured with an Agilent E5071C vector network analyzer (VNA) connected to either end of the line.

The flux crosstalk between the bias lines and the two superconducting loops must now be determined to enable independent control of f_β and f_ϵ. The system can be calibrated by measuring the periodicity of the flux through each loop. The signal transmission through the TL at a single frequency is measured as voltage is swept on both of the bias lines. Voltage applied to each line sends a current that induces flux through the two loops and tunes the qubit gap ω_{10}. When the detuning, $\delta = \omega_s - \omega_{10}$, between the signal frequency and the qubit gap approaches zero, the photons are absorbed producing a visible dip in the transmission. These dips form a closed contour when performing a 2D sweep of f_β and f_ϵ which are called frequency contours. The frequency contours occur near $(f_\beta, f_\epsilon) = (0.5 + n, 0.5 + m)$ for integer values of n and m.

The crosstalk can be evaluated as a matrix operation on the input voltages at the bias lines following the relationship

$$\begin{pmatrix} f_\beta + \frac{1}{2} \\ f_\epsilon + \frac{1}{2} \end{pmatrix} = \begin{pmatrix} W_{\beta\beta} & W_{\beta\epsilon} \\ W_{\epsilon\beta} & W_{\epsilon\epsilon} \end{pmatrix}^{-1} \begin{pmatrix} V_\beta \\ V_\epsilon \end{pmatrix} + \begin{pmatrix} V_{0,\beta} \\ V_{0,\epsilon} \end{pmatrix}, \tag{3.4}$$

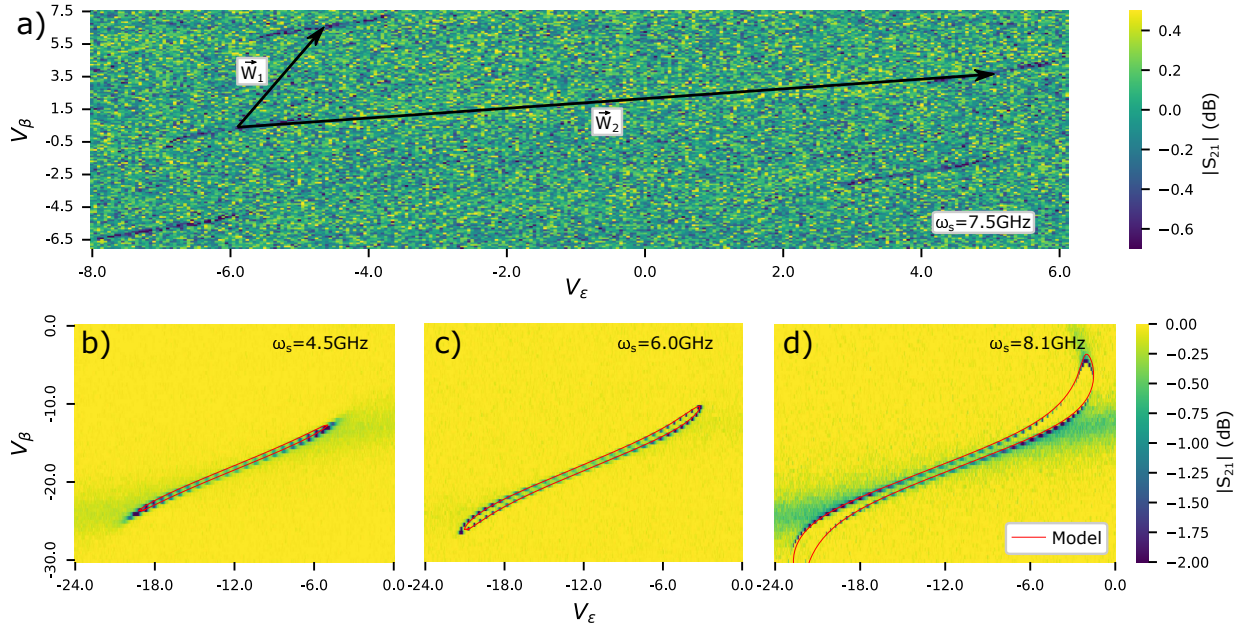

Figure 3.2: (a) $|S_{21}|$ response as a function of V_ϵ and V_β in the bias lines at 7.5 GHz showing 5 frequency contours. Two translation vectors $\vec{W}_1$ and $\vec{W}_2$ demonstrate the period of the device. The periodicity vectors are factor of 10 less than subsequent tests resulting from a smaller resistance used between the voltage source and the bias line. (b)-(d) Frequency contours of the coupler when the signal frequency ω_s is set to $4.5, 6.0, 8.1$ GHz respectively. The red line overlay shows the simulated contour after model fitting. See main text.

where f_i is the flux in each loop, W_{ij} are the elements of the crosstalk matrix, V_i are the applied voltages, and $V_{0,i}$ are the offset voltages corresponding to the circuit biased at $(f_\beta, f_\epsilon) = (0.5, 0.5)$. The crosstalk matrix was determined by scanning over a wide range of voltages, and then using an image analysis routine to determine the periodicity of the data [6]. Likewise, image inversion symmetries were used to measure the voltage offset. Fig. 3.2(a) shows the transmission through the TL for $\omega_s = 7.5$ GHz versus applied voltage as well as two extracted translation vectors $\vec{W}_1 = (W_{\beta\beta}, W_{\epsilon\beta})$ and $\vec{W}_2 = (W_{\beta\epsilon}, W_{\epsilon\epsilon})$ which demonstrate the expected periodicity of the system. The two translation vectors $\vec{W}_1$ and $\vec{W}_2$ show the bias increase by one flux quantum in the coupling and the qubit loops respectively. When extracting these vectors, high resolution images of the frequency

contours were gathered to increase accuracy. Fig. 3.2(b)-(d) shows additional scans at various frequencies that illustrate how the contours change with frequency. The frequency contours seen in these additional scans do not directly correspond to a feature in Fig. 3.2(a) due to change in the electronics setup.

With the system calibrated, transmission spectroscopy measurements can be made by sweeping f_ϵ at different values of f_β as shown in Fig. 3.3(a)-(c). Unlike standard flux qubits, $f_{\epsilon,\mathrm{sym}}$ is not generally at $f_\epsilon = 0.5$ due to an effective bias resulting from the neighbouring persistent current in the coupling loop. At $f_\beta = 0.5$, the current in the coupling loop goes to 0 and we recover a nominal PCQ where the symmetry point of the qubit loop is at $f_\epsilon = 0.5$. We can determine $f_{\epsilon,\mathrm{sym}}$ for each f_β by measuring the f_ϵ dependent qubit splitting frequency from the spectroscopy and then fitting to Eq. (3.3). As evidenced by Fig. 3.3(a)-(c), the flux in the coupling loop also impacts Δ and to a lesser extent I_p of system.

The device parameters are extracted by fitting the qubit splitting data ω_{10} to values simulated by a circuit model. The circuit model produces the qubit splitting for given flux values and predicts the coupling of the device. The model is in good agreement with the data as seen by the transmission in Fig. 3.2(b)-(d) and the qubit frequency fits of Fig. 3.3(d).

After $f_{\epsilon,\mathrm{sym}}$ is determined for each f_β value, we use these coordinates to characterize the coupling range of the device by measuring the transmission versus signal frequency and power. The transmission t follows the equation [22]

$$t = \frac{1 - r_0 + (\frac{\delta}{\gamma_{10}})^2 + 2\frac{N_{\mathrm{in}}}{\gamma_{10}} + i r_0 \frac{\delta}{\gamma_{10}}}{1 + (\frac{\delta}{\gamma_{10}})^2 + 2\frac{N_{\mathrm{in}}}{\gamma_{10}}}, \tag{3.5}$$

where $\delta = \omega_s - \Delta$ is the detuning of the signal frequency from the qubit gap, γ_{10} is the dephasing rate, $r_0 \equiv \Gamma_{10}/2\gamma_{10}$ with Γ_{10} the relaxation rate, and N_{in} is the average number of incoming photons per second. The transmission spectra were fit to extract the relaxation rates and the qubit gap as these describe the coupling strength between TLS and TL. The transmission response at different powers for $(f_\beta, f_\epsilon) = (0.41, 0.433)$ is displayed in Fig. 3.4. The data is fit globally to all powers P in dBm. For each P the parameter N_{in} is constrained to $N_{\mathrm{in}} = 10^{(P-A)/10-3}/\hbar\omega_s$ where the attenuation A is a parameter of the fit. This photon number dominates the fit when the power at the qubit exceeds the single

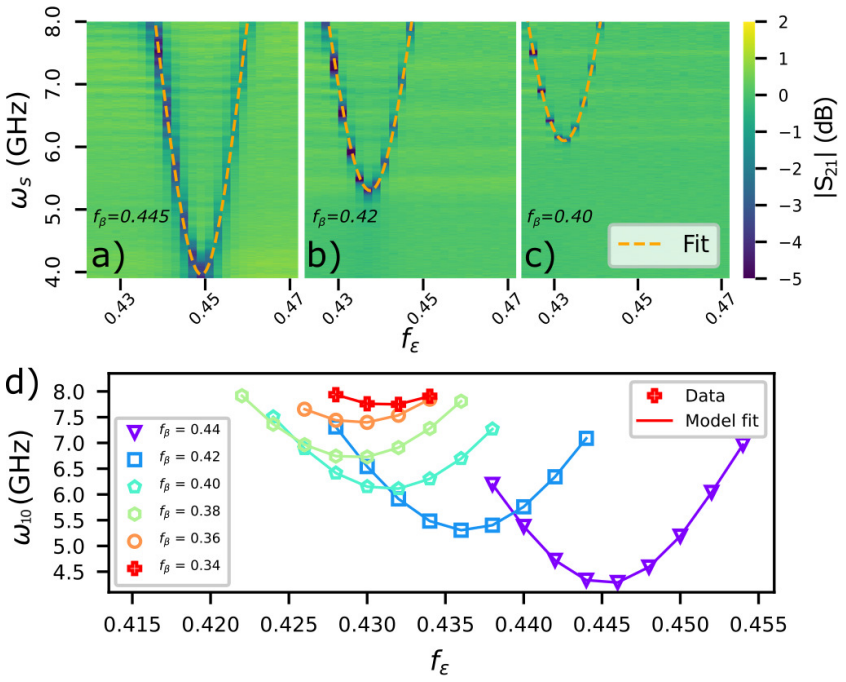

Figure 3.3: (a)-(c) Spectroscopy data measuring $|S_{21}|$ as a function of f_ϵ and ω_s at several f_β values shows changing gap frequency ω_{10} and $f_{\epsilon,\mathrm{sym}}$. The dashed line displays the fit to Eq. (3.3). (d) Fitting of the qubit gap versus f_ϵ for various f_β values using a circuit model. The qubit gap frequencies are determined by fitting the transmission peak for different coordinates of (f_β,f_ϵ).

photon regimes the start of which can be seen at $-24\ dBm$ as the transmission suppression begins to decrease.

The coupling of this tunable system can now be fully characterized as depicted in Fig. 3.5 and compared to the circuit model simulation. The data produced by the circuit model fit are shown in the solid lines and predict the behaviour of this device well. In Fig. 3.5(a) plots for both the qubit splitting Δ and $f_{\epsilon,\text{sym}}$ versus f_β are shown. The relaxation rate Γ_{01} compared to f_β is shown in Fig. 3.5(b) which can be seen to approach the qubit splitting frequency Δ. Finally, the coupling strength α is plotted in Fig. 3.5(c) following Eq. (2.29). The minimum value of $\Gamma_{01} = 37\ MHz$ is measured at $f_\beta = 0.36$ while the maximum value was measured to be $\Gamma_{01} = 1.6\ GHz$ at $f_\beta = 0.44$. These produce a range of values for α where $\alpha_{\text{min}} = 2.4 \times 10^{-4}$ and $\alpha_{\text{max}} = 1.2 \times 10^{-1}$ respectively which is an on-off ratio of 500 or 2.7 orders of magnitude.

This result demonstrates that the device is able to decouple the TLS and the TL as well as enable the USC regime at $\alpha \sim 0.1$ [8, 15]. By changing the flux bias through the coupling loop, we can effectively turn the coupling on or off based on the needs of an experiment. Furthermore, as we see from the simulated data, the coupling can be extrapolated to achieve $\alpha_{\text{max}} = 0.32$ which approaches the non-perturbative USC regime [8, 15]. The minimum coupling is likely below the experimental value as well. The dip transmission spectra for $f_{beta} \approx 0.365$ is not distinguishable from the background noise and thus no smaller coupling is measured. At this decoupling point, the interaction strength between the TL and the qubit loop is very small which causes any dip in transmission to have a very narrow width and become dominated by the residual dephasing. The total dephasing can be observed in the values of r_0 which are plotted on the inset for Fig. 3.5(b). When r_0 is close to 1, the total dephasing is dominated by relaxation of the TLS to the TL, however when r_0 is close to 0, the residual dephasing takes over. We see that near our decoupling point, the value of r_0 is very small and the residual dephasing dominates.

This device exhibits considerable control over the coupling between a TLS and a waveguide which has immediate impact in several subsequent experiments. Most fundamentally, the coupler can be used to explore the time-domain properties of USC regime of light-matter interactions. Experiments are proposed [28] where the qubit is excited, fast-tuned to the USC regime to interact with the TL for a given time, and then decoupled to readout

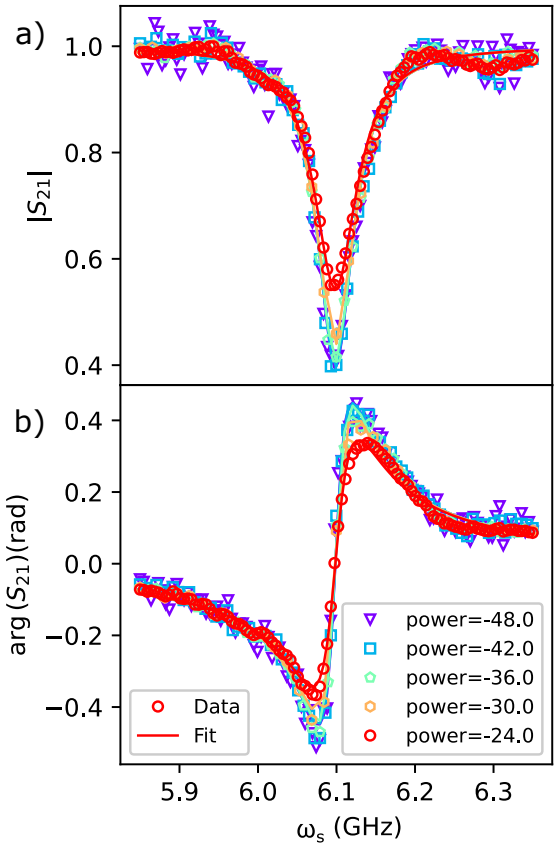

Figure 3.4: Plots of the transmission response $|S_{21}|$ versus signal frequency for multiple powers (dBm) at a symmetry point $(f_\beta, f_\epsilon) = (0.41, 0.433)$ with qubit splitting of 6.1 GHz. The power saturates near -30 dBm where the minimum transmission starts to become apparent. The peaks are fit simultaneously using Eq. (3.5) to determine the qubit gap and the relaxation rate. (a) The magnitude of the response. (b) The phase of the response.

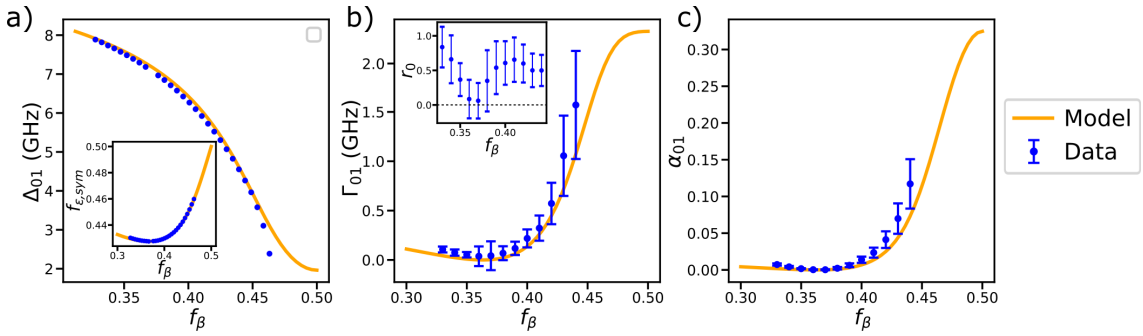

Figure 3.5: The extracted versus simulated data of key parameters for the coupled system. The measurements sweep through values of f_β while f_ϵ is tuned to ensure the qubit loop remains at its symmetry point. (a) The qubit gap frequency. The inset shows values for $f_{\epsilon,\mathrm{sym}}$. (b) The relaxation rate Γ_{01} measured by fitting spectroscopy data using Eq. (3.5). The inset displays r_0 values which are used to calculate the relaxation rate and residual dephasing of the system. (c) The coupling α_{01} between the TLS and the TL. The coupling ranges from $\alpha_{\min} = 2.1 \times 10^{-4}$ and $\alpha_{\max} = 0.098$ which shows large tunablility and entry into the USC regime.

the state. The device is designed to use fast-tuning pulses applied at the bias lines to perform this protocol which can provide direct measurement of the relaxation rate in the USC regime rather than estimates like Eq (3.5) that use the RWA. Further, the device can be used for relativistic quantum information (RQI) investigations by acting as the experimental realization of a switching function [13]. Switching functions are often implemented when making theoretical predictions in RQI, but are very challenging to implement experimentally as they essentially require instantly isolating an atom from its surroundings. This tunable coupler demonstrates the isolation of an artificial atom from its environment, and subsequent tests hope to show this can be done over very short times scales of the order of a few nanoseconds. We are also preparing an RQI test in which two of these couplers allow spatially separate qubits to interact with a single transmission line over very short time scales. With suitable initialization and fast-switching pulses, this setup holds promise for demonstrating entanglement harvesting from vacuum [24, 27]. Lastly, the device has application in photon packet production where the TLS can be excited and then coupled

to the TL using a fast pulse to generate versatile shaped single photons [12, 9].

In summary, we describe and implement a system whereby a TLS is tunably coupled to a waveguide from a decoupling point up to the USC regime. The two superconducting loops can be calibrated to account for flux crosstalk using the periodic nature inherent in PCQs. The spectroscopic data is used to determine the symmetry points of the system and the qubit splitting frequencies are in very good agreement with our modelling. Finally. the transmission at the symmetry points is fit to characterize coupling strength between the TLS and the waveguide. The tunable coupler can be applied to a broad range of experiments that demand the controlled interaction between a qubit and a waveguide.

Chapter 4

Conclusion

4.1 Summary

We presented in this thesis a tunable coupler that is able to mediate light-matter interactions from a decoupled state to the ultra-strong coupling (USC) regime. Light-matter interactions are well described by the spin-boson model. However, typical approximations such as the rotating wave approximation (RWA) begin to break down as the coupling increases into the USC regime. Achieving this regime enables explorations into the fundamental physics of these intense interactions and relativistic quantum information (RQI) experiments. In order to tune the coupling strength and enter the USC regime, we showed that artificial atoms can be coupled to a bosonic bath in a superconducting circuit. The coupling is controlled using a quantum inductance that mediates an effective mutual inductance between the persistent current qubit (PCQ) and the transmission line (TL) which can be used to tune their interaction strength into the USC regime.

Unlike previous coupler systems within superconducting circuits, the device we presented has the key advantage of having a large tunablility and being able decouple the two-level system (TLS) from the transmission line. This tunability is achieved using a PCQ as a coupling loop that, when biased with an external magnetic flux, controls the interaction strength between the TLS and the TL.

The tunable coupler device uses two bias lines to control the flux through both the qubit loop and the coupling loop. The proximity of these two loops results in large flux crosstalk between them that must be accounted for when operating the system. The crosstalk was successfully calibrated by measuring the periodicity of the two superconducting loops with respect to the voltage applied at each bias line. After calibration, the symmetry points were measured from spectroscopy data gathered for a range of flux bias values in the coupling loop. At each symmetry point, the transmission through the TL was measured at several powers and the response data was fit in order to extract the coupling strength. The final results of this investigation showed that the interaction strength generated by this tunable coupler ranges from $\alpha_{\min} = 2.4 \times 10^{-4}$ to $\alpha_{\max} = 1.2 \times 10^{-1}$.

4.2 Outlook

With the successful demonstration of the USC regime in a tunable coupler capable of also decoupling the system, our next goal is to perform time-domain measurements of the qubit dynamics in the USC regime. The tunable coupler can be used to directly measure the relaxation rate, the dephasing rate, and the tunneling frequency of the TLS. In the USC regime, the interactions occur on such small time scales, that it is challenging to measure them while the system is in the USC regime. Instead, the measurement protocols rely on letting the state evolve in the USC regime and then decoupling the system to freeze the qubit state for measurement.

The tunable coupler device opens new research directions in RQI by realizing an experimental switching function. Experiments proposed for RQI require very fast, short interactions between an artificial atoms and a TL that are only achievable in the USC regime with a fast-tunable coupler. A superconducting circuit that uses two of the tunable coupler devices has been designed to perform this experiment in the near future.

References

[1] Aji A. Anappara, Simone De Liberato, Alessandro Tredicucci, Cristiano Ciuti, Giorgio Biasiol, Lucia Sorba, and Fabio Beltram. Signatures of the ultrastrong light-matter coupling regime. *Physical Review B*, 79(20):201303, May 2009. Publisher: American Physical Society.

[2] J. Bardeen, L. N. Cooper, and J. R. Schrieffer. Microscopic Theory of Superconductivity. *Physical Review*, 106(1):162–164, April 1957. Publisher: American Physical Society.

[3] Félix Beaudoin, Jay M. Gambetta, and A. Blais. Dissipation and ultrastrong coupling in circuit QED. *Physical Review A*, 84(4):043832, October 2011. Publisher: American Physical Society.

[4] Alec Maassen van den Brink, A J Berkley, and M Yalowsky. Mediated tunable coupling of flux qubits. *New Journal of Physics*, 7:230–230, November 2005.

[5] John Clarke and Frank K. Wilhelm. Superconducting quantum bits. *Nature*, 453(7198):1031–1042, June 2008. Number: 7198 Publisher: Nature Publishing Group.

[6] X. Dai, D.M. Tennant, R. Trappen, A.J. Martinez, D. Melanson, M.A. Yurtalan, Y. Tang, S. Novikov, J.A. Grover, S.M. Disseler, J.I. Basham, R. Das, D.K. Kim, A.J. Melville, B.M. Niedzielski, S.J. Weber, J.L. Yoder, D.A. Lidar, and A. Lupascu. Calibration of Flux Crosstalk in Large-Scale Flux-Tunable Superconducting Quantum Circuits. *PRX Quantum*, 2(4):040313, October 2021. Publisher: American Physical Society.

[7] Guillermo Díaz-Camacho, Alejandro Bermudez, and Juan José García-Ripoll. Dynamical polaron Ansatz: A theoretical tool for the ultrastrong-coupling regime of circuit QED. *Physical Review A*, 93(4):043843, April 2016. Publisher: American Physical Society.

[8] P. Forn-Díaz, J. J. García-Ripoll, B. Peropadre, J.-L. Orgiazzi, M. A. Yurtalan, R. Belyansky, C. M. Wilson, and A. Lupascu. Ultrastrong coupling of a single artificial atom to an electromagnetic continuum in the nonperturbative regime. *Nature Physics*, 13(1):39–43, January 2017.

[9] P. Forn-Díaz, C.W. Warren, C.W.S. Chang, A.M. Vadiraj, and C.M. Wilson. On-Demand Microwave Generator of Shaped Single Photons. *Physical Review Applied*, 8(5):054015, November 2017. Publisher: American Physical Society.

[10] Austin G. Fowler, William F. Thompson, Zhizhong Yan, Ashley M. Stephens, B. L. T. Plourde, and Frank K. Wilhelm. Long-range coupling and scalable architecture for superconducting flux qubits. *Physical Review B*, 76(17):174507, November 2007. Publisher: American Physical Society.

[11] Oliver Heaviside. XIX. *On the extra current. The London, Edinburgh, and Dublin Philosophical Magazine and Journal of Science*, 2(9):135–145, August 1876.

[12] A. A. Houck, D. I. Schuster, J. M. Gambetta, J. A. Schreier, B. R. Johnson, J. M. Chow, L. Frunzio, J. Majer, M. H. Devoret, S. M. Girvin, and R. J. Schoelkopf. Generating single microwave photons in a circuit. *Nature*, 449(7160):328–331, September 2007. Number: 7160 Publisher: Nature Publishing Group.

[13] B L Hu, Shih-Yuin Lin, and Jorma Louko. Relativistic quantum information in detectors–field interactions. *Classical and Quantum Gravity*, 29(22):224005, November 2012.

[14] E.T. Jaynes and F.W. Cummings. Comparison of quantum and semiclassical radiation theories with application to the beam maser. *Proceedings of the IEEE*, 51(1):89–109, January 1963. Conference Name: Proceedings of the IEEE.

[15] Anton Frisk Kockum, Adam Miranowicz, Simone De Liberato, Salvatore Savasta, and Franco Nori. Ultrastrong coupling between light and matter. *Nature Reviews Physics*, 1(1):19–40, January 2019. arXiv: 1807.11636.

[16] Anton Frisk Kockum, Adam Miranowicz, Vincenzo Macrì, Salvatore Savasta, and Franco Nori. Deterministic quantum nonlinear optics with single atoms and virtual photons. *Physical Review A*, 95(6):063849, June 2017. Publisher: American Physical Society.

[17] A. J. Leggett, S. Chakravarty, A. T. Dorsey, Matthew P. A. Fisher, Anupam Garg, and W. Zwerger. Dynamics of the dissipative two-state system. *Rev. Mod. Phys.*, 59(1):1–85, January 1987. Publisher: American Physical Society.

[18] T. Niemczyk, F. Deppe, H. Huebl, E. P. Menzel, F. Hocke, M. J. Schwarz, J. J. Garcia-Ripoll, D. Zueco, T. Hümmer, E. Solano, A. Marx, and R. Gross. Circuit quantum electrodynamics in the ultrastrong-coupling regime. *Nature Physics*, 6(10):772–776, October 2010. Number: 10 Publisher: Nature Publishing Group.

[19] A. O. Niskanen, K. Harrabi, F. Yoshihara, Y. Nakamura, S. Lloyd, and J. S. Tsai. Quantum Coherent Tunable Coupling of Superconducting Qubits. *Science*, 316(5825):723–726, May 2007. Publisher: American Association for the Advancement of Science.

[20] T. P. Orlando, J. E. Mooij, Lin Tian, Caspar H. van der Wal, L. S. Levitov, Seth Lloyd, and J. J. Mazo. Superconducting persistent-current qubit. *Physical Review B*, 60(22):15398–15413, December 1999. Publisher: American Physical Society.

[21] B. Peropadre. Nonequilibrium and Nonperturbative Dynamics of Ultrastrong Coupling in Open Lines. *Physical Review Letters*, 111(24), 2013.

[22] B Peropadre, J Lindkvist, I-C Hoi, C M Wilson, J J Garcia-Ripoll, P Delsing, and G Johansson. Scattering of coherent states on a single artificial atom. *New J. Phys.*, 15(3):035009, March 2013.

[23] B. L. T. Plourde, J. Zhang, K. B. Whaley, F. K. Wilhelm, T. L. Robertson, T. Hime, S. Linzen, P. A. Reichardt, C.-E. Wu, and John Clarke. Entangling flux qubits with a bipolar dynamic inductance. *Physical Review B*, 70(14):140501, October 2004. Publisher: American Physical Society.

[24] Alejandro Pozas-Kerstjens and Eduardo Martín-Martínez. Harvesting correlations from the quantum vacuum. *Physical Review D*, 92(6):064042, September 2015. Publisher: American Physical Society.

[25] E. M. Purcell. Spontaneous emission probabilities at radio frequencies. *Physical Review Journals*, 69:674–674, June 1946.

[26] G. Romero, D. Ballester, Y. M. Wang, V. Scarani, and E. Solano. Ultrafast Quantum Gates in Circuit QED. *Physical Review Letters*, 108(12):120501, March 2012. Publisher: American Physical Society.

[27] Grant Salton, Robert B. Mann, and Nicolas C. Menicucci. Acceleration-assisted entanglement harvesting and rangefinding. *New Journal of Physics*, 17(3):035001, March 2015. Publisher: IOP Publishing.

[28] Jiahao Shi. Fast Switchable Ultrastrong Coupling Between Superconducting Artificial Atoms and Electromagnetic Fields. August 2019. Accepted: 2019-08-23T15:25:58Z Publisher: University of Waterloo.

[29] A. Wallraff, D. I. Schuster, A. Blais, L. Frunzio, R.-S. Huang, J. Majer, S. Kumar, S. M. Girvin, and R. J. Schoelkopf. Strong coupling of a single photon to a superconducting qubit using circuit quantum electrodynamics. *Nature*, 431(7005):162–167, September 2004. Number: 7005 Publisher: Nature Publishing Group.

[30] Yimin Wang, Chu Guo, Guo-Qiang Zhang, Gangcheng Wang, and Chunfeng Wu. Ultrafast quantum computation in ultrastrongly coupled circuit QED systems. *Scientific Reports*, 7(1):44251, March 2017. Number: 1 Publisher: Nature Publishing Group.

[31] Steven J. Weber. Coherent Coupled Qubits for Quantum Annealing. *Physical Review Applied*, 8(1), 2017.

[32] U. Weiss. Quantum dissipative systems (series in modern condensed matter physics; v. 13). In *Quantum Dissipative Systems*, pages 1–4. World Scientific, May 2008.

APPENDICES

Appendix A

Circuit Model Description for the Tunable Coupler

The tunable coupler device we introduce consists of a two-loop flux qubit galvanically coupled to an open transmission line as shown in Fig. 3.1(a). The TLS is generated in the first loop called the qubit loop. The qubit loop consists of a 4-junction PCQ with an external flux bias $f_\epsilon = \Phi_{\epsilon,\text{ext}}/\Phi_0$ that couples to the transmission line through the quantum inductance of the coupling loop. The coupling loop is 3-qubit PCQ with an external flux bias $f_\beta = \Phi_{\beta,\text{ext}}/\Phi_0$. To maximize the mutual inductance, junctions 4 and 5 of the coupling loop are connected to the qubit-loop and the waveguide respectively.

As with other flux qubits, the flux through the superconducting loops is quantized and follows a relation based on the phase of the junctions. The two loops are constrained by

$$\begin{aligned} \gamma_1 + \gamma_2 + \gamma_3 + \gamma_4 + 2\pi f_\epsilon &= 0, \\ \gamma_4 + \gamma_5 + \gamma_6 - 2\pi f_\beta &= 0, \end{aligned} \tag{A.1}$$

where γ_i is the phase across junction i. The circuit can be solved using the same Hamiltonian formulation as the PCQ in Eq. 2.20 so we have

$$H = \frac{1}{2\varphi_0^2}\boldsymbol{p}^T\tilde{C}^{-1}\boldsymbol{p} + U, \tag{A.2}$$

where $\tilde{C}$ is the capacitance matrix, $\boldsymbol{p}$ is the momentum vector, and U is the potential energy stored in system. We can use Eq. A.1 to constrain the potential so that we are left with only 4 degrees of freedom. Thus we are left with the potential

$$\begin{aligned} U = -\phi_0[&I_{c1}cos\gamma_2 + I_{c1}cos\gamma_2 + I_{c3}cos(\gamma_1 + \gamma_2 + \gamma_3 + 2\pi f_\epsilon) \\ &+ I_{c4}cos\gamma_4 + I_{c5}cos\gamma_5 + I_{c6}cos(\gamma_4 + \gamma_5 - 2\pi f_\beta)]. \end{aligned} \tag{A.3}$$

The capacitance matrix C and momentum $\boldsymbol{p}$ are similarly constrained to 4 degrees of freedom.

The Hamiltonian is numerically generated as a matrix by using Eq A.2. The momentum coordinates are introduced into the model using the relation

$$p_i = \hbar n_i. \tag{A.4}$$

where n_i is the charge number on each island of the circuit. The maximum number of charges is be restricted to a small number to decrease the size of matrix that needs to be solved. The Hamiltonian is diagonalized to find the the qubit frequency at symmetry Δ and the relaxation rates Γ_{01}. With this model, the circuit can be simulated and optimized for our experiment. Circuit parameters are chosen such that the qubit frequencies are within the operation range of our setup and the tunable coupler enables coupling in the USC regime.